Comparison of multiple Kalman filter and moving horizon estimator for the anesthesia process

Bob Aubouin–Pairault, Mirko Fiacchini, Thao Dang

Comparison of Multiple Kalman Filter and Moving Horizon Estimator for the Anesthesia Process

Aubouin–Pairault Bob [1a,b], Fiacchini Mirko[a], Dang Thao[b]

[a] *Univ. Grenoble Alpes, CNRS, Grenoble INP, GIPSA-lab, , Grenoble, 38000, , France*
[b] *Univ. Grenoble Alpes, CNRS, Grenoble INP, VERIMAG, , Grenoble, 38000, , France*

Abstract

In this paper, a new method to estimate the states and the parameters of the anesthesia process is proposed and compared to a Moving Horizon Estimator (MHE) approach. The proposed method makes use of multiple extended Kalman filters (MEKF) where each EKF uses a different set of system parameters whose selection is based on a predictive performance criterion. In view of usage in a closed loop, the comparison between the two methods is based on a metric quantifying the capability of the estimators to predict the future behavior of the system. The metric is also used as a performance measure for tuning the hyperparameters of the estimators. While the results on simulated data are similar, the MEKF method outperforms MHE on clinical data. Tests show that the MEKF method can better predict the future trajectory of the system during the whole induction, on average for all the patients but also for the worst scenario.

Keywords: Anesthesia, multiple Kalman filter, moving horizon estimator, extended observability.

1. Introduction

The field of anesthesia, an indispensable facet of modern medicine, has undergone remarkable advancements over the years. Its primary objective is to render patients insensible to pain during surgery or other medical procedures, ensuring their comfort and well-being. Anesthesiologists, equipped with an array of powerful pharmacological agents, have the task of inducing hypnosis (lack of consciousness), analgesia (lack of pain), and muscle relaxation in addition to ensuring the stability of hemodynamic and respiratory variables.

The control of drugs administered during these procedures is fundamental for the success of anesthesia. Achieving the delicate balance between ensuring patient safety and maintaining precise control over the depth of anesthesia is a paramount challenge. With the advent of quick-acting intravenous drugs like propofol and remifentanil, and the use of EEG-based hypnotic indicators such as the bispectral index (BIS), researchers have been exploring the possibility of automating the drug delivery process [1], [2].

Since the beginning of the century, many closed-loop methods have been proposed to control drug rates during general anesthesia. As some of them have been tested in clinical trials, metastudies agree on the benefits of such methods compared to manual control [3], [4]. Nevertheless, some issues are still to be appropriately addressed before such methods can be used in clinical routine [5]. In fact, the huge uncertainties due to the intra- and inter-patient variability along with the high level of reliability required for this application are still relevant challenges.

Control methods often rely on a model of the patient's response to the drugs, either for tuning the controller, *e.g.* PID methods [6], or to be directly employed in the controller, *e.g.* MPC methods [7]. For intravenous drugs such as propofol and remifentanil, compartment models are used to describe the pharmacokinetics (PK) of drugs and surface models are used to describe the pharmacodynamics (PD) of the drugs [8]. The PK-PD model is often used to predict the effect of the drugs on the patient. Such a model takes the drug rates as inputs and the BIS (bispectral index) value as output. The BIS is an indicator of hypnosis which varies between 0 and 100 where 100 means a fully awake state while 0 stands for a flat EEG. A desired BIS value during general anesthesia is in the interval $[40, 60]$. The main issue affecting the existing models is the uncertainties associated with the models, in [9] the more recent models are associated with a median absolute predictive error of 20%. To tackle this issue, models specific to clinical situations have been proposed, in [10] to model drug trapping in long-term anesthesia and in [11] to model the effect of blood loss on the PK-PD model for instance. However, those models are still subject to uncertainties and cannot capture the diversity of events happening during surgical procedures.

Online parameter identification, on the other hand, could be a solution to individualize the model for each patient. If this solution is often used in control applications, some requirements are specific to its application to general anesthesia. In fact, the identification must be fast enough to allow the controller to compute the optimal drug dose. It should also be robust enough to ensure patient safety. Online parameter identification has already been studied, in particular for estimating the PD parameters, as they are the most sensitive parameters of the system [12]. In [13] and [14] the parameters of the PD

models are identified periodically by solving a least square optimization problem for the propofol to BIS system. In [15] the parameters of a reduced propofol-remifentanil to BIS system are estimated. Recently, in [16], a Moving Horizon Estimator was proposed to estimate both the states and the PD parameters of propofol-remifentanil to BIS system. However, when using this method in closed-loop, it appears that this approach does not converge fast enough to ensure safe regulation of anesthesia during the first minutes of the procedure.

The aim of this paper is to propose a method to estimate both system states and parameters in order to be able to predict the future trajectory of the system. As those estimators are intended to be used in a predictive control context for regulating the output value, the main objective is the identification of a model able to predict the future evolution of the output, rather than the real value of the states, not accessible in practice. To do so, an approach based on multiple Kalman filters is proposed and compared to a Moving Horizon Estimator. The different Kalman filters use different values of the PD parameters to estimate the states of the system. Choosing one Kalman filter results in practice in choosing a set of PD parameters and states. This discrete approach to the estimation problem for the PD parameters has been motivated by the poor observability of the system, which leads to slow convergence of the parameter estimates in standard estimation methods. The switching between the Kalman filters is based on the method analogous to the one proposed in [17]. The method is compared to the Moving Horizon Estimator, first using data obtained by simulating the uncertain model using known distributions of the parameters in both the PK and the PD models, and then using real data from the VitalDB dataset [18].

This paper is organized as follows. Section 2 recalls the standard PK-PD model of anesthesia and discusses the observability of the extended system. Section 3 explains the details of the proposed method and the metrics used to evaluate the performance. The results on simulated data are presented in Section 4 and those on clinical data in Section 5. Finally, some conclusions are presented in Section 6.

2. Anesthesia Model

Drug models involved in anesthesia dynamics are usually composed of two parts: the Pharmacokinetic (PK) and the Pharmacodynamic (PD). The PK model describes the dynamics of the drug concentrations in the patient's body, whereas the PD represents the link between the drug concentrations and their physiological effects.

2.1. Compartments Pharmacokinetic Model

For pharmacokinetic (PK) models of both drugs, propofol and remifentanil, a common approach is to use a four compartment model. This model divides the body into three physical compartments: blood, muscles, and fat; and a virtual effect site, as illustrated in Fig. 1. The compartment model results in a linear system represented by the following equations:

$$\begin{pmatrix}\dot{x}_1\\ \dot{x}_2\\ \dot{x}_3\\ \dot{x}_4\end{pmatrix} = \begin{pmatrix}-(k_{10}+k_{12}+k_{13}) & k_{12} & k_{13} & 0\\ k_{21} & -k_{21} & 0 & 0\\ k_{31} & 0 & -k_{31} & 0\\ k_e & 0 & 0 & -k_e\end{pmatrix}\begin{pmatrix}x_1\\ x_2\\ x_3\\ x_4\end{pmatrix} + \begin{pmatrix}\frac{1}{V_1}\\ 0\\ 0\\ 0\end{pmatrix} u \tag{1}$$

where x_1, x_2, x_3, and x_4 represent respectively the drug concentrations in blood, muscle, fat, and effect-site. The coefficients can be determined from Eq. (2) below, except for k_e which is not related to a physical meaning:

$$k_{10} = \frac{Cl_1}{V_1}, k_{12} = \frac{Cl_2}{V_1}, k_{13} = \frac{Cl_3}{V_1}, k_{21} = \frac{Cl_2}{V_2}, k_{31} = \frac{Cl_3}{V_3} \tag{2}$$

with V_i and Cl_i ($i = 1, 2, 3$) respectively the volume and the clearance rates of each compartment, which can be computed from a population-based model as in [19] and [20]. The input u is the drug infusion rate. Next, the notation x_p and x_r for the states of the compartment model for propofol and remifentanil is used. Also, A_p, B_p, A_r, and B_r are the state and input matrices of both drugs. Finally, both compartment models can be described by the decoupled system:

$$\begin{pmatrix}\dot{x}_p\\ \dot{x}_r\end{pmatrix} = \begin{pmatrix}A_p & 0^{4\times4}\\ 0^{4\times4} & A_r\end{pmatrix}\begin{pmatrix}x_p\\ x_r\end{pmatrix} + \begin{pmatrix}B_p & 0^{4\times1}\\ 0^{4\times1} & B_r\end{pmatrix}\begin{pmatrix}u_p\\ u_r\end{pmatrix}. \tag{3}$$

2.2. Pharmacodynamic Model

The impact of the drug concentrations on the bispectral index (BIS) is typically modeled by a Hill function. Due to the synergy between propofol and remifentanil, the effect can be modeled as a response surface model [21]:

$$y(t) = BIS(t) = E_0\left(1 - \frac{U(t)^\gamma}{1 + U(t)^\gamma}\right) \tag{4}$$

with E_0 the initial BIS, γ the slope coefficient of the surface and $U(t)$ the interaction term defined by:

$$U(t) = \frac{x_{p4}(t)}{C_{50p}} + \frac{x_{r4}(t)}{C_{50r}}. \tag{5}$$

In these equations, x_{p4} and x_{r4} are the propofol and remifentanil concentrations of the effect-site, C_{50p} and C_{50r} are the propofol and remifentanil half-effect concentrations for BIS (*i.e.* the concentrations to obtain half of the effect of the drugs).

Finally, the fully discretized model subject to noise can be summarized by the following structure:

$$\begin{cases} x(k+1) = Ax(k) + Bu(k)\\ y(k) = h(x(k)) + w(k)\end{cases} \tag{6}$$

where h is the non-linear output function from Eq. (4)-(5) and w models both the measurement noise and the eventual output disturbances.

In the simulation, the parameters of [22] and [23] are used respectively for propofol and remifentanil PK model. For the

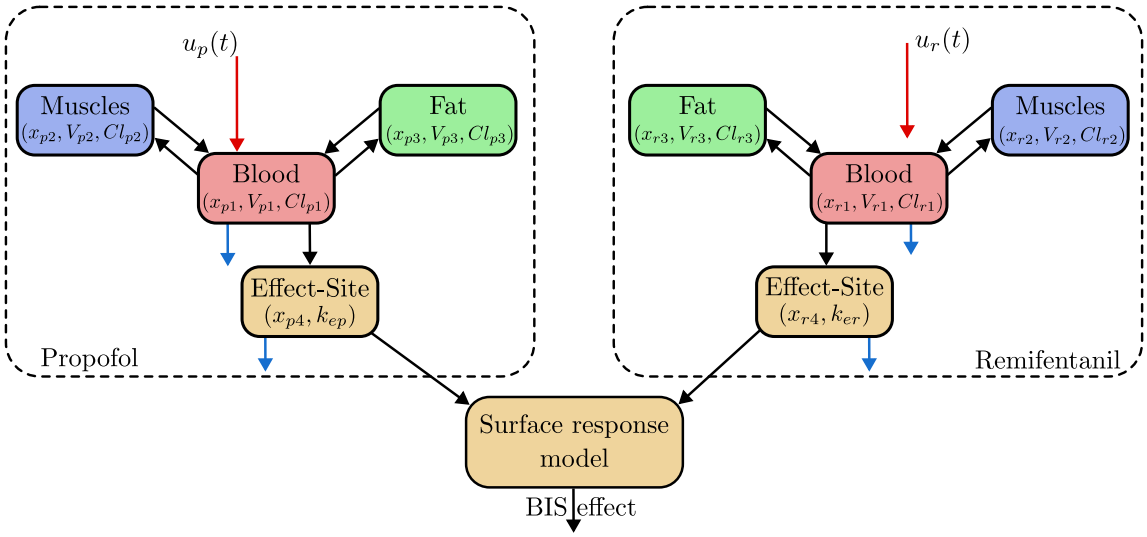

Figure 1: Schemes of the PK-PD compartments model

PD model, the parameters from [24] are implemented.

To have simulations as close to reality as possible, uncertainties are added to the parameters. Particularly, each parameter uncertainty follows a log-normal distribution (the parameters of this distribution are specified in the previously cited papers), and a realization of the distribution is used for each patient. In practice, for each simulated patient, first a nominal model $(A_{nom}, B_{nom}, h_{nom})$ is computed using patient demography data and then uncertainties are introduced to obtain the simulated model $(A_{sim}, B_{sim}, h_{sim})$. This way of modeling the inter-patient variability allows the estimator to have access only to the nominal model and not to the simulated one.

2.3. *Extended observability of the system*

The goal of this paper is to compare two methods for estimating both the states and the PD parameters. The parameter E_0 can be measured before the induction of anesthesia and E_{max} is usually set equal to E_0. Thus, the remaining parameters are C_{50p}, C_{50r}, and γ, hence $\theta = (C_{50p},\ C_{50r},\ \gamma)$ is used to describe the vector of unknown parameters. As the PD parameters are not accessible, an extended system must be considered here. The extended state is given by $\bar{x} = (x,\ \theta)$ with the dynamics:

$$\begin{cases} \bar{x}(k+1) = \bar{A}\bar{x}(k) + \bar{B}u(k) \\ y(k) = \bar{h}(\bar{x}(k)), \end{cases} \tag{7}$$

with $\bar{A} = \begin{pmatrix} A & 0_{8\times3} \\ 0_{3\times8} & I_{3\times3} \end{pmatrix}$ and $\bar{B} = \begin{pmatrix} B \\ 0_{3\times2} \end{pmatrix}$. $\bar{h}$ is the output function h of the system parameterized by the PD parameters θ inside the extended state $\bar{x}$.

In order to analyze the observability of the system, we consider the continuous time version of the dynamics. Given a standard non-linear system of dimension N:

$$\begin{aligned} \dot{x} &= f(x,u) \\ y &= h(x), \end{aligned}$$

The observability matrix ([25]) is defined by:

$$\mathcal{O} = \begin{pmatrix} \frac{\partial h}{\partial x} & \frac{\partial L_{f_u} h}{\partial x} & \frac{\partial L_{f_u}^2 h}{\partial x} & \dots & \frac{\partial L_{f_u}^{N-1} h}{\partial x} \end{pmatrix}$$

where L_{f_u} is the Lie derivative along f_u defined by:

$$L_{f_u} h = \frac{\partial h}{\partial x} f(x,u)$$

Using a formal calculation software, one can conclude that the observability matrix is full rank for the system (7) when the states are non-null. This guarantees the structural observability of the system. However, as this is a non-linear framework, the persistent excitation of the system condition must be ensured to guarantee the practical observability of the system. To verify this condition, the empirical observability Gramian can be computed as in [26]. This matrix is positive semi-definite if the persistent excitation of the system is verified. Moreover, the higher the eigenvalues are, the faster the estimator will be able to converge. For system (7), the minimal eigenvalue of the Gramian matrix for 10 closed-loop simulations (defined later in Section 4.1) is computed. A mean value of approximately $2.1 \times 10^{-7} \pm 3.01 \times 10^{-8}$ is obtained. For comparison, the same simulation with null inputs leads to a value of zero, and input amplitude divided by 100 leads to a value of $1.4 \times 10^{-7} \pm 4.4 \times 10^{-8}$, which shows that the system is weakly-excited. This means that the excitation of the system is nearly sufficient to have observability, but the convergence will be quite slow.

Note that this study on the observability assumes that $\bar{A}$ and $\bar{B}$ are known. In practice, though, uncertainties are present in these matrices, which leads to a harder problem. All these considerations imply that it is almost impossible to accurately estimate the extended state vector. However, as the end goal is to use an estimator in a closed-loop process, it is sufficient that the identified model can reasonably predict the future behavior of the system. This is why the metric used to compare the

estimators (described in Section 3.3) does not consider the convergence of the states.

3. Methods

In this section, different methods used to estimate the unknown parameters of the PD models are detailed.

The Multiple Extended Kalman Filter (MEKF) method selects the best vector in a grid over the space of the parameters. This discrete choice allows a fast convergence but less precise at the end. The Moving Horizon Estimation (MHE) method uses an extended state formulation to estimate the vector of parameters along with the state in a continuous space. Thus, the method could identify more precisely the parameters but is more subject to noise and could be slower than MEKF.

3.1. Multiple Extended Kalman Filter

In order to identify the PD parameters, the MEKF method uses a set of extended Kalman filter (EKF), one for every realization of the vector selected within a grid in the space of the parameters. The grid is designed to reasonably represent the variability of the parameter vector. Then, the active vector is chosen using a model-matching criterion. Fig. 2 illustrates the principle of the method.

EKF is a state-estimation method that relies on the linearization of a non-linear model. If we consider the model given in Eq. (6) with the non-linear function h parametrized by θ, the estimator using the parameter vector θ^i is given by:

$$
\begin{aligned}
H^i(k) &= \left.\frac{\partial h(x,\theta^i)}{\partial x}\right|_{x=\hat{x}^i(k|k-1)} \\
K^i(k) &= P^i(k|k-1)H^{i\top}(k)\Big(H^i(k)P^i(k|k-1)H^{i\top}(k) + R_2\Big)^{-1} \\
\hat{x}^i(k|k) &= \hat{x}^i(k|k-1) + K^i(k)\Big(y(k) - h(\hat{x}^i(k|k-1),\theta^i)\Big) \\
P^i(k|k) &= P^i(k|k-1) - K^i(k)H^i(k)P^i(k|k-1) \\
\hat{x}^i(k+1|k) &= A\hat{x}^i(k|k) + Bu(k) \\
P^i(k+1|k) &= AP^i(k|k)A^\top + R_1
\end{aligned}
$$

where, the notation $X(k_1|k_2)$ represents the value of variable X computed at time step k_1 based on the knowledge available at k_2, and X^i denotes the variable associated to the parameter vector θ^i. The estimated state vector is $\hat{x}^i$ and P^i is the covariance matrix. A and B are the matrices describing the discretized dynamic system, Eq. (6). R_1 and R_2 are two constant matrices used to respectively characterize the process uncertainties and the measurements noise. Notice that in the Kalman filter the assumption that process uncertainty can be modeled by additive process noises is implicitly made. For the studied system, though, the process uncertainty comes from the matrix parameters which is different. However, as demonstrated later, this assumption is sufficient to obtain an estimator able to estimate coherent states, and to satisfactorily predict the future trajectory of the system.

This method aims at selecting the 'best' observer at each time step, by using the criterion proposed in [17]. In [17], this criterion has been proposed to choose an estimator between different Luenberger estimators using different gains. The novelty here is to use this same criterion to select the best EKF among a set of EKF using different system parameters.

To evaluate the criterion for each observer, the estimation error on the output is $e^i(k) = y(k) - h(x(k|k-1),\theta^i)$, computed at each time step. The dynamics of the criterion for the i^{th} observer is then given by:

$$\eta^i(k+1) = \nu\eta^i(k) + \lambda_1|e^i(k)|^2 + \lambda_2|K^i(k)e^i(k)|^2, \tag{8}$$

where λ_1, λ_2, and ν are three positive hyper-parameters. The criterion depends both on the output estimation error $e^i(k)$ and the correction effort of the observer $K_i(k)e^i(k)$. The following equation can be deduced from Eq. (8):

$$\eta^i(k) = \nu^k\eta^i(0) + \sum_{j=1}^{k}\nu^{k-j-1}(\lambda_1|e^i(j)|^2 + \lambda_2|K^i(j)e^i(j)|^2). \tag{9}$$

where η^i can be seen as a cost, permitting to select the observer with the minimal cost at each time step. The index of the currently selected observer is denoted by i^*. The parameter ν is a forgetting factor; a small value of ν giving more importance to the last error value but leading to bigger fluctuation of the EKF choice. The ratio $\frac{\lambda_1}{\lambda_2}$ should be of the same magnitude as K^i in order to give similar importance to the estimation error and the correction effort.

To avoid too many switches between the observers, the parameter $\epsilon \in (0, 1]$ is introduced, and the switch takes place at time step k only if it exists $i \neq i^*$ such that $\eta^i(k) < \epsilon\eta^{i^*}(k)$. A small value of ϵ will lead to a more stable behavior of the filter, although, it will degrade the performance as the selected EKF will not always be the one with the smallest criterion.

To initialize the criterion of each observer, $\eta^i(0)$ is set to reflect the prior probability of θ^i on the grid to be close to the real θ.

3.2. Moving Horizon Estimation

In order to include the estimation of θ along the state estimation, the MHE method uses an extended state formulation. The extended system and its dynamics have been described in Eq. (7) and an MHE method has been already presented and tested in [16]. In this paper, a different MHE formulation has been employed to meet the standard formulation given by:

$$
\begin{aligned}
&\min_{\bar{\mathbf{x}}(k)} \quad J_N(\bar{\mathbf{x}}(k), \hat{\bar{\mathbf{x}}}(k-1), \mathbf{y}, \mathbf{u}) \\
&\text{s.t.} \qquad x \in \mathbb{X}
\end{aligned}
\tag{10}
$$

where $\mathbb{X}$ is the set of admissible state values (only positive values for our system) and the cost function is given by:

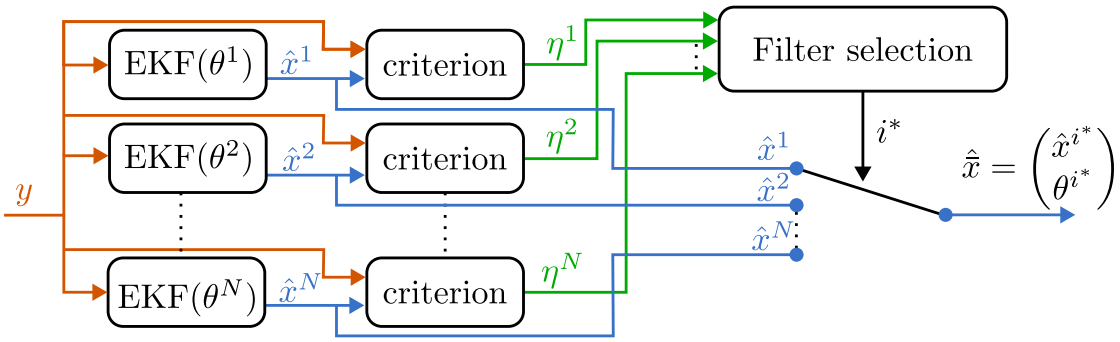

Figure 2: Block diagram of the Multiple Extended kalman filter Estimator, adapted from [17].

$$J_N(\bar{\mathbf{x}}(k), \hat{\bar{\mathbf{x}}}(k-1), \mathbf{y}, \mathbf{u}) = \sum_{i=k-N_{MHE}}^{k} \|y(i) - \bar{h}(\bar{x}(i))\|_R$$
$$+ \sum_{i=k-N_{MHE}+1}^{k} \|\bar{x}(i) - (\bar{A}\bar{x}(i-1) + \bar{B}u(i-1))\|_Q$$
$$+ \|\bar{x}(k-N_{MHE}) - \hat{\bar{x}}(k-N_{MHE})\|_P$$

where $\bar{\mathbf{x}}(k), \hat{\bar{\mathbf{x}}}(k-1), \mathbf{y}, \mathbf{u}$, respectively represent the state vector up to time k and the previously estimated state up to time $(k-1)$ over the estimation horizon, the output, and the input measurements over the estimation horizon. Q and P are two positive semi-definite matrices used to penalize the deviation from the model dynamics and the previous state estimation, R is a positive scalar used to penalize the output error, and N_{MHE} is the length of the horizon. These four constants are used as hyper-parameters.

3.3. Metric for the comparison

At first, simulated data was used to compare the two methods. In this setup, all simulation parameters and states are known and a simple way to evaluate the performance of the estimators could have been to compare the estimated states and parameters with the true ones. However, this idea will lead to inaccurate results. In fact, since the dynamics are different in the simulation and in the estimators due to the introduction of uncertainties ((A_{sim}, B_{sim}) for simulation and (A_{nom}, B_{nom}) for the observers, as discussed in Section 2.2), the identified parameters that better reproduce the observed behavior might not be equal to those used for simulation. Nevertheless, as the comparison between the estimations and the measured values is aimed at predicting the BIS value, the capability of the estimators to predict in open-loop the BIS value in the near future is considered as performance measure.

The idea, illustrated in Fig. 3, is to perform, at some instants, an open-loop simulation of the system starting from the estimated states and parameters and to compare the output of the simulation with the actual output. The metric used to compare the different methods is the mean square error (MSE) between the actual output and the simulated one. The MSE is computed over the next two minutes after the end of the estimation. This time length might be, for instance, related to the

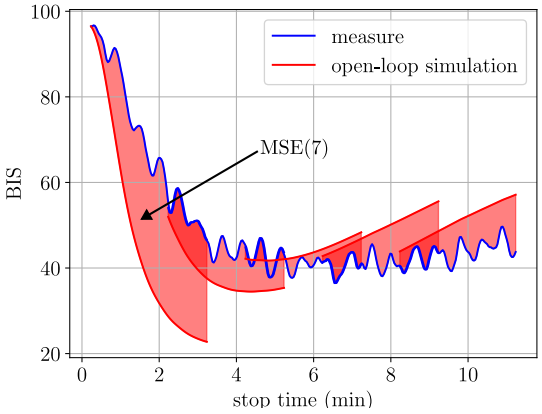

Figure 3: Illustration of the proposed metric

MPC prediction horizon in a control framework. Thus, the metric computed at time step k is given by:

$$\text{MSE}(k) = \sum_{i=k}^{k+N_{MSE}} \left(y(i) - \bar{h}(\hat{\bar{x}}_k(i))\right)^2, \tag{11}$$

where N_{MSE} is the number of samples in two minutes, and $\hat{\bar{x}}_k(i)$ is the extended state value computed in open-loop starting from the state estimation $\hat{\bar{x}}(k)$ at time step k:

$$\begin{cases} \hat{\bar{x}}_k(i+1) = \bar{A}_{nom}\hat{\bar{x}}_k(i) + \bar{B}_{nom}u(i) \\ \hat{\bar{x}}_k(k) = \hat{\bar{x}}(k) \end{cases} \tag{12}$$

4. Tests on simulated data

Consider first the tuning of the estimators and the analysis on simulated data.

4.1. Data generation

To obtain a simulated dataset representative of clinical data, a PID controller already proposed in [6] has been used. For this control method, the ratio between propofol and remifentanil rates is fixed to 2. Then a PID controller is used to control the rates using the BIS signal. An example of the resulting control is represented in Fig. 4.

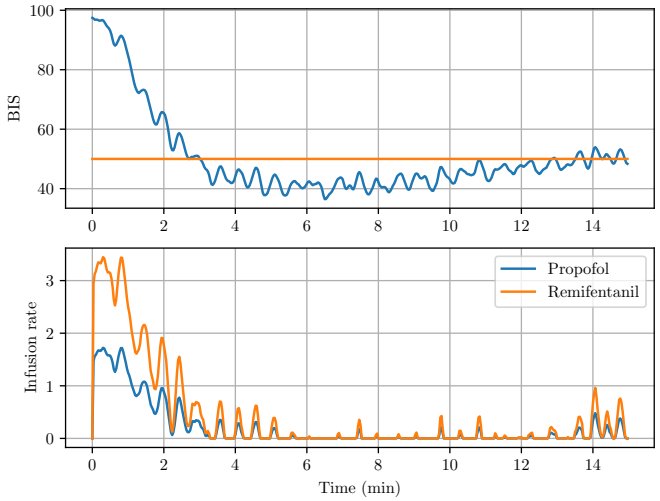

Figure 4: Results of the control algorithm for a single random patient.

The final database includes induction (15 minutes) simulation files for 500 different patients, with a sampling time of two seconds. Patient features have been randomly chosen using uniform distribution (age $\in$ [18, 70], height $\in$ [150, 190], weight $\in$ [50, 100], and gender $\in$ {0, 1}). The parameters of the PK-PD models were randomly chosen according to the distributions from [22], [23] and [24]. Noise has been added to the output as white noise (standard deviation of 3) filtered by a second-order low-pass filter with a cut-off frequency of 0.03 Hz. Fig. 5 shows the results of the simulations for the 500 patients. Simulations are done using the Python Anesthesia Simulator [27], Python code for data generation and estimators comparison is available on Github (`https://github.com/BobAubouin/MEKF_vs_MHE`).

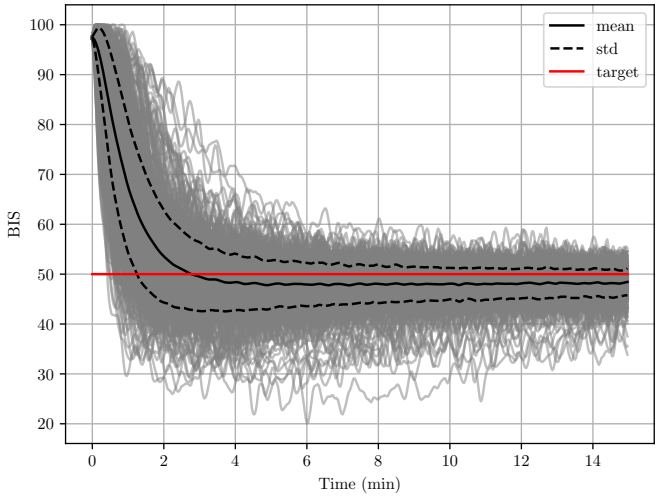

Figure 5: BIS trajectory for all the simulations.

4.2. *Tuning of the parameters*

Tuning of the hyperparameters can be an arduous task for observers. In order to obtain a fair comparison between the methods, a single metric was used to tune the hyperparameters of the observers. This metric is the integral of the mean square error, as computed in Eq. (11). More precisely, the parameters were tuned to minimize the following cost function:

$$f = \frac{1}{N_{patient}} \sum_{k=0}^{N_{patient}} \sum_{i=0}^{N_{sim}-N_{MSE}} \mathrm{MSE}_k(i), \tag{13}$$

where $N_{patient}$ is the number of patients considered for the tuning (16 random patients from the simulated database), N_{sim} the duration of the simulation (15 minutes), $MSE_k(i)$ the MSE computed at time step i for the patient k.

A tree-structured parzen estimator algorithm [28] was used to tune the main hyper-parameters of the observers. For the MHE, four hyper-parameters were investigated: the horizon N_{MHE}, the penalty scalar R, a scalar q such that $Q = q \times Q_{const}$ where Q_{const} is a given matrix and the value of β used in the penalty matrix P as follows:

$$P = \begin{pmatrix} P_1 & 0 \\ 0 & \beta P_2 \end{pmatrix}, \tag{14}$$

where $P_1 \in \mathbb{R}^{8\times8}$ and $P_2 \in \mathbb{R}^{3\times3}$ are the penalty matrices for the state and the parameters respectively, tuned to obtain a similar rate of convergence for each variable. The best results are obtained with $R = 2.36\times10^{-4}$, $\beta = 4.35\times10^{-4}$, and the estimation horizon $N_{MHE} = 26$.

For the MEKF, the grid of the parameters has been fixed using the known distribution. More precisely, the interval [0,1] is linearly partitioned into n equal parts, where n is the number of different parameter values in the grid ($n = 5$ for C_{50p} and $n = 6$ for C_{50r} and for γ). Then, each value is evaluated using the percent point function (inverse of the cumulative distribution function) as illustrated in Fig. 6. The grid is the combination of all the possible values of each parameter, leading to 180 points.

For the optimization, four hyper-parameters were investigated: the penalty matrix R_1 and a multiplicative coefficient for R_2 matrix in the Kalman filters, the value of λ_2 in the computation of the criterion in Eq. (8) and the value of ϵ for the

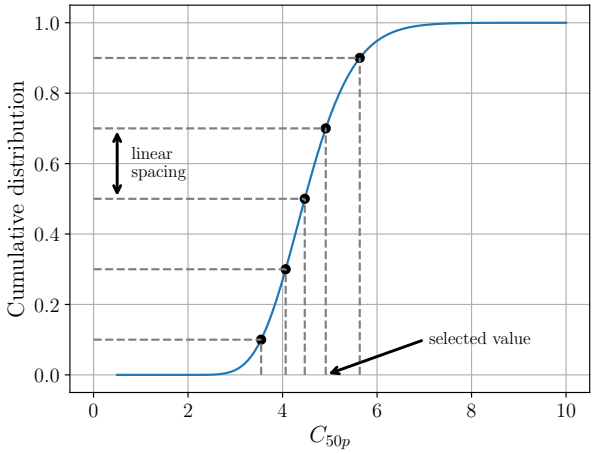

Figure 6: Illustration of the parameters value choice for the grid construction.

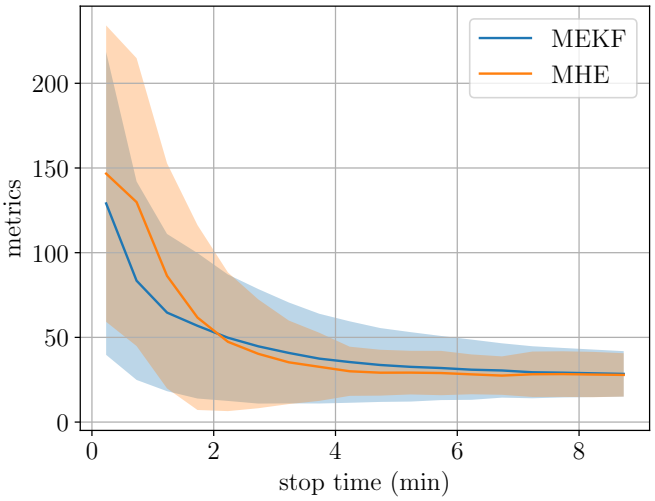

Figure 7: Comparison of the metrics at different time steps for the two methods on simulated data. Mean value and standard deviation are given.

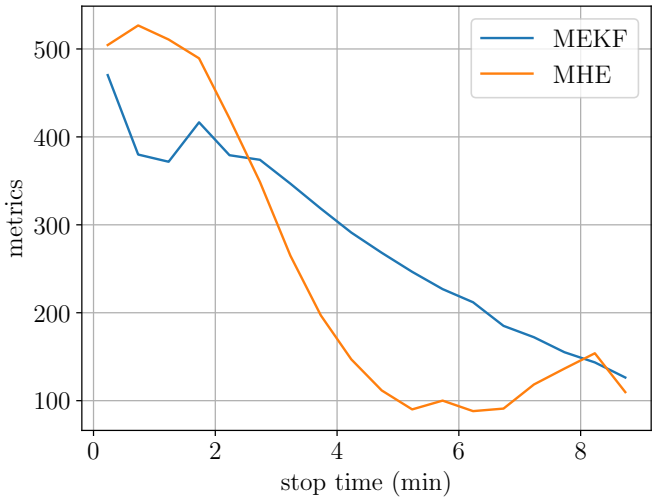

Figure 8: Maximum of the metrics at different time steps for the two methods on simulated data.

switching rule. Parameters ν and λ_1 were set respectively to 10^{-5} and 1, a small value of ν allowing the criterion not to forget the past error, while the value of λ_1 is fixed since only the ratio λ_1/λ_2 is relevant. The best results have been obtained with $R_1 = 76.5$, $\lambda_2 = 3.33$, $\epsilon = 0.76$, and $R_2 = 0.058 \times diag([0.1, 0.1, 0.05, 0.05, 1, 1, 10, 1])$.

4.3. Results

The results over the 500 simulated patients are shown in Fig. 7. One can observe that both methods have similar metric curves. The MEKF seems to converge faster during the first 2 minutes, but then the MHE is more precise. At the end of the simulation, the two methods converge to the same mean value. Concerning the spread of the curves, after 2 minutes the standard deviation of MHE is smaller than the one of MEKF (as for the mean value), finally converging to the same value. These results might be explained by the proper structure of each method. The MEKF employs a discrete grid of parameter values, while MHE uses a continuous approximation of the parameters. Thus, the MEKF can converge faster but less precisely than the MHE. While a smaller final value for the MHE was expected, both estimators in reality converge to the same value.

Considering the worst-case results, Fig. 8 shows the maximum of the metrics for each method. The same performances are obtained as for the mean metrics. It should be noted, however, that the difference between the MHE and MEKF after 2 minutes is greater than for the mean value.

Concerning the computation times, the MEKF method is faster than the MHE, with a mean iteration time of 50ms for the MEKF and 130ms for the MHE. Both are suitable for a real-time implementation, as the sampling time is 2 seconds. However, the fact that the MEKF is faster is interesting, since the computation of the Kalman filters could be done in parallel to accelerate the process.

Overall, the results of both methods are fairly similar and do not demonstrate a clear superiority of one method. Moreover, these results are still dependent on the tuning of the controller and particularly on the choice of the grid for the MEKF. One can imagine that a finer grid could help the MEKF method converge to a better mean precision at the price of a higher computational burden.

5. Tests on clinical data

Clinical data selection and results analysis are presented hereafter.

5.1. Data description

The methods were also tested using a clinical dataset, namely a subset of the vitalDB dataset [18]. This recent repository is the first open-source perioperative high-resolution database, it involves 6388 surgical patients and is composed of intraoperative biosignals and clinical information. The data used in this paper is composed of 188 patients undergoing general anesthesia. Cases with only propofol and remifentanil were selected, and a visual inspection of the data was done to ensure the consistency of the signals. The data was resampled to 0.5Hz and the first 15 minutes, from the first injection, was used for the study. This is justified by the fact that this period corresponds to the ones with lower disturbances, as the surgery has not started yet.

5.2. Results

Statistical results of the estimations with different methods are presented in Fig. 9 and are obtained using the same parameters as in the previous section for both estimators. The estimators could have been tuned again to better fit the clinical data, however, the goal is to test the robustness of the method on new data. Thus, both methods perform worse on this set of data

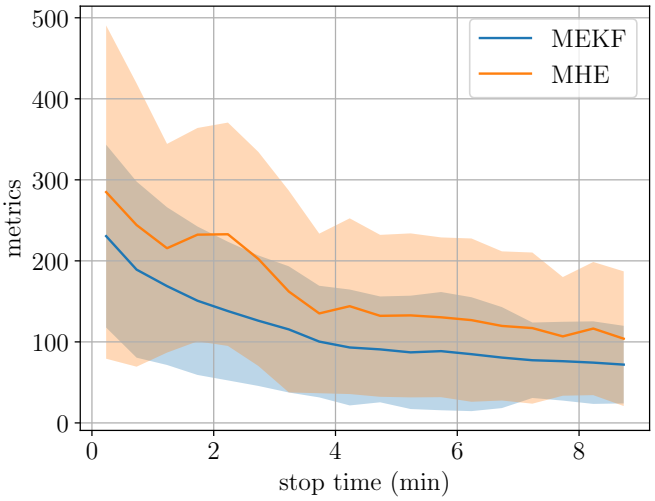

Figure 9: Comparison of the metrics at different time steps for the two methods on clinical data. Mean value and standard deviation are given.

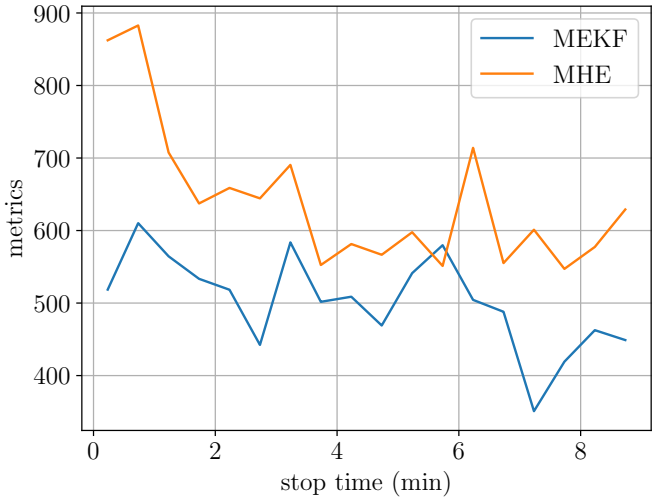

Figure 10: Maximum of the metrics at different time steps for the two methods on clinical data.

than on the simulated data. The results are different from those obtained on simulated data (Fig. 7). On the clinical data, the MEKF estimator performs better than the MHE during all the simulations. Both the mean value and the associated standard deviation are smaller. This demonstrates the robustness of the MEKF on real-world data. This might be explained by the fact that the discrete approach of the parameter estimation is less affected by the noise and the disturbances present in the clinical data.

The maximum values for the metrics are available in Fig. 10 for both methods. Here the MEKF is also better than the MHE during almost all the simulations. Overall, compared to the results on simulated data, the MEKF method performs better than MHE when using the methods on clinical data. This could be explained by the fact that this method uses a grid of parameters, which is more robust than a continuous approach for the estimation as in the MHE. This grid approach is less likely to lead to incoherent and unstable parameter estimation.

6. Conclusion

This paper proposes a new estimation method, based on multiple extended Kalman filters, and a comparison with the classical MHE two methods to estimate both the states and the PD parameters of a PK-PD system during general anesthesia. For the comparison, both observers have been tuned using the same criteria, which evaluate the ability of the estimators to predict the future output of the system. Using the same metric, tests on simulated data show that both methods have similar behavior, converging to the same final value with different profiles. However, while using the same parameter for the tests on clinical data, the MEKF method performs better than the MHE. This suggests that a discrete approach to parameter identification provides robustness to the estimation.

Future work will focus on using a combination of both methods to propose a closed-loop control of the anesthesia process. Moreover, the approach could be applied to other applications, where a fast and robust estimation of system parameters is required.

Acknowledgment

This work has been partially supported by the LabEx PERSYVAL Lab (ANR-11-LABX-0025-01) funded by the French program Investissement d'avenir.

References

[1] D. Copot, *Automated Drug Delivery in Anesthesia*. Academic Press, 2020.

[2] M. Ilyas, M. F. U. Butt, M. Bilal, K. Mahmood, A. Khaqan, and R. Ali Riaz, "A Review of Modern Control Strategies for Clinical Evaluation of Propofol Anesthesia Administration Employing Hypnosis Level Regulation," *BioMed Research International*, vol. 2017, p. e7432310, Mar. 2017.

[3] E. Brogi, S. Cyr, R. Kazan, F. Giunta, and T. M. Hemmerling, "Clinical Performance and Safety of Closed-Loop Systems: A Systematic Review and Meta-analysis of Randomized Controlled Trials," *Anesthesia & Analgesia*, vol. 124, pp. 446–455, Feb. 2017.

[4] L. Pasin, P. Nardelli, M. Pintaudi, M. Greco, M. Zambon, L. Cabrini, and A. Zangrillo, "Closed-Loop Delivery Systems Versus Manually Controlled Administration of Total IV Anesthesia: A Meta-analysis of Randomized Clinical Trials," *Anesthesia & Analgesia*, vol. 124, pp. 456–464, Feb. 2017.

[5] M. Ghita, M. Neckebroek, C. Muresan, and D. Copot, "Closed-Loop Control of Anesthesia: Survey on Actual Trends, Challenges and Perspectives," *IEEE Access*, vol. 8, pp. 206264–206279, 2020.

[6] M. Schiavo, F. Padula, N. Latronico, M. Paltenghi, and A. Visioli, "Individualized PID tuning for maintenance of general anesthesia with propofol and remifentanil coadministration," *Journal of Process Control*, vol. 109, pp. 74–82, Jan. 2022.

[7] I. Naşcu, A. Krieger, C. M. Ionescu, and E. N. Pistikopoulos, "Advanced Model-Based Control Studies for the Induction and Maintenance of Intravenous Anaesthesia," *IEEE Transactions on Biomedical Engineering*, vol. 62, pp. 832–841, Mar. 2015.

[8] C. M. Ionescu, M. Neckebroek, M. Ghita, and D. Copot, "An Open Source Patient Simulator for Design and Evaluation of Computer Based Multiple Drug Dosing Control for Anesthetic and Hemodynamic Variables," *IEEE Access*, vol. 9, pp. 8680–8694, 2021.

[9] B. Aubouin-Pairault, M. Fiacchini, and T. Dang, "Data-based Pharmacodynamic Modeling for BIS and Mean Arterial Pressure Prediction during General Anesthesia," in *2023 European Control Conference (ECC)*, pp. 1–6, June 2023.

[10] D. Copot and C. Ionescu, "Tailored Pharmacokinetic model to predict drug trapping in long-term anesthesia," *Journal of Advanced Research*, vol. 32, pp. 27–36, Sept. 2021.

[11] M. Ghita, D. Copot, I. Birs, C. Muresan, M. Neckebroek, and C. Ionescu, "Modelling of Blood Loss Influence on Propofol Concentrations and Anesthetic States in Critical Responses *," in *2023 American Control Conference (ACC)*, pp. 2216–2221, May 2023.

[12] A. Krieger, N. Panoskaltsis, A. Mantalaris, M. C. Georgiadis, and E. N. Pistikopoulos, "Modeling and Analysis of Individualized Pharmacokinetics and Pharmacodynamics for Volatile Anesthesia," *IEEE Transactions on Biomedical Engineering*, vol. 61, pp. 25–34, Jan. 2014.

[13] I. Martín-Mateos, J. Méndez Pérez, J. Reboso Morales, and J. Gómez-González, "Adaptive pharmacokinetic and pharmacodynamic modelling to predict propofol effect using BIS-guided anesthesia," *Computers in Biology and Medicine*, vol. 75, pp. 173–180, Aug. 2016.

[14] M. M. da Silva, T. Mendonça, and T. Wigren, "Online nonlinear identification of the effect of drugs in anaesthesia using a minimal parameterization and BIS measurements," in *Proceedings of the 2010 American Control Conference*, pp. 4379–4384, June 2010.

[15] R. D. Keyser, D. Copot, and C. Ionescu, "Estimation of Patient Sensitivity to Drug Effect during Propofol Hypnosis," in *2015 IEEE International Conference on Systems, Man, and Cybernetics*, pp. 2487–2491, Oct. 2015.

[16] K. Moussa, B. Aubouin-Pairault, M. Alamir, and T. Dang, "Data-Based Extended Moving Horizon Estimation for MISO Anesthesia Dynamics," *IEEE Control Systems Letters*, vol. 7, pp. 3054–3059, 2023.

[17] E. Petri, R. Postoyan, D. Astolfi, D. Nešić, and V. Andrieu, "Towards improving the estimation performance of a given nonlinear observer: A multi-observer approach," in *2022 IEEE 61st Conference on Decision and Control (CDC)*, pp. 583–590, Dec. 2022.

[18] H.-C. Lee, Y. Park, S. B. Yoon, S. M. Yang, D. Park, and C.-W. Jung, "VitalDB, a high-fidelity multi-parameter vital signs database in surgical patients," *Scientific Data*, vol. 9, p. 279, June 2022.

[19] T. W. Schnider, C. F. Minto, S. L. Shafer, P. L. Gambus, C. Andresen, D. B. Goodale, and E. J. Youngs, "The Influence of Age on Propofol Pharmacodynamics," *Anesthesiology*, vol. 90, pp. 1502–1516., June 1999.

[20] C. F. Minto, T. W. Schnider, T. D. Egan, E. Youngs, H. J. M. Lemmens, P. L. Gambus, V. Billard, J. F. Hoke, K. H. P. Moore, D. J. Hermann, K. T. Muir, J. W. Mandema, and S. L. Shafer, "Influence of Age and Gender on the Pharmacokinetics and Pharmacodynamics of Remifentanil: I. Model Development," *Anesthesiology*, vol. 86, pp. 10–23, Jan. 1997.

[21] C. F. Minto, T. W. Schnider, T. G. Short, K. M. Gregg, A. Gentilini, and S. L. Shafer, "Response Surface Model for Anesthetic Drug Interactions," *Anesthesiology*, vol. 92, pp. 1603–1616, June 2000.

[22] D. J. Eleveld, P. Colin, A. R. Absalom, and M. M. R. F. Struys, "Pharmacokinetic–pharmacodynamic model for propofol for broad application in anaesthesia and sedation," *British Journal of Anaesthesia*, vol. 120, pp. 942–959, May 2018.

[23] D. J. Eleveld, J. H. Proost, H. Vereecke, A. R. Absalom, E. Olofsen, J. Vuyk, and M. M. R. F. Struys, "An Allometric Model of Remifentanil Pharmacokinetics and Pharmacodynamics," *Anesthesiology*, vol. 126, pp. 1005–1018, June 2017.

[24] T. W. Bouillon, J. Bruhn, L. Radulescu, C. Andresen, T. J. Shafer, C. Cohane, and S. L. Shafer, "Pharmacodynamic Interaction between Propofol and Remifentanil Regarding Hypnosis, Tolerance of Laryngoscopy, Bispectral Index, and Electroencephalographic Approximate Entropy," *Anesthesiology*, vol. 100, pp. 1353–1372, June 2004.

[25] G. Besançon, *Nonlinear Observers and Applications*. No. 363 in Lecture Notes in Control and Information Sciences, Berlin Heidelberg: Springer, 2007.

[26] A. J. Krener and K. Ide, "Measures of unobservability," in *Proceedings of the 48h IEEE Conference on Decision and Control (CDC) Held Jointly with 2009 28th Chinese Control Conference*, (Shanghai, China), pp. 6401–6406, IEEE, Dec. 2009.

[27] B. Aubouin-Pairault, M. Fiacchini, and T. Dang, "PAS: A Python Anesthesia Simulator for drug control," *Journal of Open Source Software*, vol. 8, p. 5480, Aug. 2023.

[28] T. Akiba, S. Sano, T. Yanase, T. Ohta, and M. Koyama, "Optuna: A Next-generation Hyperparameter Optimization Framework," in *Proceedings of the 25th ACM SIGKDD International Conference on Knowledge Discovery & Data Mining*, KDD '19, (New York, NY, USA), pp. 2623–2631, Association for Computing Machinery, July 2019.